

# Eccentric Phase Crossover from Thermalization to Dynamical Localization in Long-Range Many-Body Spin Systems using Floquet Engineering

Mahbub Rahaman,<sup>1</sup> Takashi Mori,<sup>2</sup> and Analabha Roy<sup>1</sup>

<sup>1</sup>*Department of Physics, The University of Burdwan, Golapbag, Bardhaman - 713 104, India*  
<sup>2</sup>*RIKEN CEMS, 2-1 Hirosawa, Wako, Saitama, 351-0198, Japan*

The phenomenon of many-body localization occurs in quantum systems under specific resonance conditions, preventing thermalization and allowing the system to maintain its initial state. Quantum dynamical localization has been validated for multi-body spin systems under the influence of transverse field. The validation has been parameterized by the Inverse Participation ratio (IPR) of Floquet modes. Power-law dependence with long-range. The study applied  $J_{ij} = 1/|i - j|^\beta$  and examined the short-range Transverse Field Ising Model for  $\beta = \infty$  and the long-range Lipkin Meshkov-Glick (LMG) model for  $\beta = 0$  at varying drive frequencies. The Ising model displays complete localization at high frequencies, while localization persists at low frequencies at the localization point. At the resonance point of system localization, LMG exhibits high-frequency localization in the long-range scenario. However, at lower frequencies, localization deteriorates following an inverse system size law. Chaos and regularity alternate at different frequencies in LMG at the phase-space continuum limit. IPR for LMG is evolved by an adiabatic increase in drive frequencies; the IPR rises gradually up to unity thereby manifesting a phase crossover which proposes a future protocol for the MBL engine.

Periodically driven Quantum Many Body Systems can experience Dynamical Freezing (DMF) when dynamical hysteresis stops observables from reaching their diagonal averaged values and thermalizing to infinite temperature [1–3]. Under certain resonance conditions in the drive parameters, DMF can cause the response to ‘freeze’ completely to its initial value at all times. This arises as a consequence of additional approximate symmetries that occur at resonance. DMF has been demonstrated via the Rotating Wave Approximation (RWA) in the driven TFIM with nearest neighbour interactions [4] and is shown to be protected when translational invariance is explicitly broken (say, by disorder) [5, 6].

In this article, we propose that this symmetry is preserved in quantum many body systems with lower symmetry such as those with long-range interactions. To demonstrate this, we investigate the driven Lipkin-Meshkov-Glick (LMG) model, a long-range system that is a special case of the more general Curie-Weiss model, wherein the nearest-neighbour exchange in the TFIM is extended to longer ranges with a power law dependence,  $J_{ij} \sim 1/|i - j|^\beta$  [7–9]. Setting  $\beta = \infty$  recovers the TFIM, and setting  $\beta = 0$  yields the LMG model. We have recovered the onset of DMF in this system and have supported our result with numerical simulations.

In addition, we compare the degree of localization of the quasi-stationary Floquet modes in both limits of  $\beta$ . In order to do so, we look at the Inverse Participation Ratio (IPR) of the Floquet modes in the representation given by the eigenstates of the symmetry-breaking field. The Inverse Participation Ratio (IPR) [10] a parameter is a useful tool for defending the many-body localization of a quantum system. For a Many-Body Localized (MBL) system, the IPR is unity, and it scales inversely with the system size when it is thermally distributed [11].

In the first section of this paper, we presented a brief overview of essential theoretical frameworks. Our results

for the LMG model are presented next in section II. In that section, we have used the Rotating Wave Approximation (RWA) [12], where only the slowest rotating terms in the Fourier expansion of the Hamiltonian in a frame co-rotating with symmetry breaking drive field are retained. In addition, we have the obtained Floquet modes and their IPR. They are used to probe the system dynamics in the high and low-frequency domains at both limits of  $\beta$ . In section III we have contrasted the classical Lipkin model driven with both at a higher frequency and sufficient lower frequency for phase-space and Husimi Q-functions analysis. In section IV we have discussed the system dynamics driven by adiabatically increased drive frequency from low to high limit thereby we propose a phase crossover in frequency domain at any fixed system localization resonance point. Finally, we conclude and discuss the outlook.

## I. BACKGROUND

The Floquet Eigenstate Thermalization Hypothesis (FETH) is a theoretical construct that characterizes the thermalization process of a quantum system that is subject to a time-periodic many-body Hamiltonian. The framework presented enables comprehension of the thermal-like behavior exhibited by a system that is intrinsically out of equilibrium. The Floquet Engineering Theorem (FETH) holds significant relevance in the investigation of stimulated quantum systems, wherein the Hamiltonian undergoes periodic fluctuations over time.

To understand FETH, let’s consider a many-body system described by a time-periodic Hamiltonian  $H(t)$  with a period  $T$ . The time evolution of the system is governed by the Schrödinger equation,  $i\hbar \frac{\partial \psi(t)}{\partial t} = H(t)\psi(t)$ , where  $\psi(t)$  is the state vector of the system at time  $t$ .

The Floquet theorem states that for a time-periodic

Hamiltonian, the solutions of the Schrödinger equation can be written as  $|\psi(t)\rangle = e^{-i\epsilon t/\hbar} |\phi(t)\rangle$ , where  $|\phi(t)\rangle$  is a T-periodic function and “ $\epsilon$ ” is the quasienergy. The quasienergy spectrum is bounded within a range of  $[-\hbar\omega/2, \hbar\omega/2]$ , where  $\omega = 2\pi/T$  is the driving frequency.

FETH posits that subject to specific conditions and in the context of a system of significant size, the quasienergy eigenstates of a time-periodic Hamiltonian exhibit thermal state-like behavior. In the context of quantum mechanics, it is possible to estimate the expectation value of an observable A in a quasienergy eigenstate  $\psi_\alpha$  with quasienergy  $\epsilon_\alpha$  by utilizing the thermal expectation value:

$$\langle \psi_\alpha | \hat{A} | \psi_\alpha \rangle = \frac{\text{Tr}(Ae^{-\beta H_{eq}})}{\text{Tr}(e^{-\beta H_{eq}})} \quad (1)$$

where  $\beta = 1/(k_B T)$  is the inverse temperature,  $H_{eq}$  is an effective Hamiltonian that captures the long-time average dynamics of the system, and  $k_B$  is the Boltzmann constant.

To put it simply, the findings of FETH propose that the many-body Hamiltonian with time-periodic characteristics undergoes thermalization over an extended period, with the quasienergy eigenstates bearing resemblance to thermal states. The aforementioned hypothesis serves as a valuable instrument for comprehending the conduct of stimulated quantum systems and their correlation with thermal equilibrium.

The Eigenstate Thermalization Hypothesis (ETH) is a conjecture that relates the expectation values of observables in individual eigenstates of a quantum system to the predictions of statistical mechanics. The derivation of ETH involves the assumption of ergodicity, which states that a system explores all accessible states in its phase space uniformly over time. Consider a many-body quantum system described by a time-dependent periodic Hamiltonian  $H(t)$  with a period T. The Schrödinger equation governing the time evolution of the system is given by  $i\hbar \frac{\partial \psi(t)}{\partial t} = \hat{H}(t) |\psi(t)\rangle$

$i\hbar \frac{\partial \psi(t)}{\partial t} = \hat{H}(t) |\psi(t)\rangle$ , where  $|\psi(t)\rangle$  is the state vector of the system at time t. We aim to derive ETH by examining the expectation value of an observable  $\hat{A}$  in an eigenstate of the Hamiltonian.

Let  $|n(t)\rangle$  be an eigenstate of  $\hat{H}(t)$  with energy  $E_n(t)$ , such that  $H(t)|n(t)\rangle = E_n(t)|n(t)\rangle$ . We want to calculate the expectation value of the observable  $\hat{A}$  in this eigenstate:  $\langle \hat{A}(t) \rangle_n = \langle n(t) | \hat{A}(t) | n(t) \rangle$ .

To proceed with the derivation, we invoke the concept of adiabatic perturbation theory, assuming that the Hamiltonian slowly varies in time. We can expand the eigenstate and eigenenergy as perturbative series:

$$|n(t)\rangle = |n(\theta)\rangle + \sum_m c_m(t) |m(\theta)\rangle,$$

$$E_n(\theta) = E_n(\theta) + \sum_m E_m(t) c_m(t)$$

where  $|m(\theta)\rangle$  represents the unperturbed eigenstates of  $H(\theta)$  with energy  $E_m(\theta)$ . The coefficients  $c_m(t)$  describe the time-dependent amplitude of the expansion. Plugging these expansions into the expression for the expectation value, we obtain:

$$\begin{aligned} \langle \hat{A}(t)_n \rangle &= \sum_{m,k} c_M^*(t) c_k(t) \langle n(\theta) | m(\theta) \rangle \\ &\quad \langle m(t) | \hat{A}(t) | k(t) \rangle \langle k(\theta) | n(\theta) \rangle \end{aligned} \quad (2)$$

where  $\langle m(t) | \hat{A}(t) | k(t) \rangle$  represents the matrix element of the observable  $\hat{A}$  between the time-dependent states  $|m(t)\rangle$  and  $|k(t)\rangle$ . In the ergodic hypothesis, it is assumed that the system explores the entire Hilbert space uniformly, such that the matrix elements  $\langle m(t) | \hat{A}(t) | k(t) \rangle$  become indistinguishable for most pairs of m and k. This allows us to approximate  $\langle m(t) | \hat{A}(t) | k(t) \rangle \approx A_{eq} \delta_{mk}$ , where  $A_{eq}$  is the expectation value of the observable  $\hat{A}$  in the equilibrium thermal ensemble. Applying this approximation, the expression for the expectation value becomes:

$$\langle \hat{A}(t) \rangle_n = \sum_m |c_m(t)|^2 \langle n(\theta) | m(\theta) \rangle \hat{A}_{eq} \langle n(0) | m(0) \rangle$$

Finally, assuming that the initial state  $|n(0)\rangle$  is random and uncorrelated with the Hamiltonian eigenstates, we can use the property  $\langle n(0) | m(0) \rangle = \delta_{nm}$ . This yields:

$$\langle \hat{A}(t) \rangle_n = \sum_m |c_m(t)|^2 \hat{A}_{eq} = \hat{A}_{eq}$$

Therefore, in the limit of large systems and under the ergodic assumption, the expectation value of an observable A in an eigenstate of the time-dependent Hamiltonian is approximately equal to the thermal expectation value  $A_{eq}$ . This is the essence of the Eigenstate Thermalization Hypothesis, which suggests that individual eigenstates of a quantum system can be described by statistical mechanics in the long-time limit.

If the system is strobed at integer multiples of the time period T, Floquet Theory allows us to obtain *quasi-stationary states* (stationary only at integer multiples of time period T) from the eigendecomposition of the Floquet Hamiltonian  $\hat{H}_F \equiv \hat{H}(T) - i\frac{\partial}{\partial t}|_T$  (see, for instance, [13, 14] and references therein). In that case, the ETH introduced by Heisenberg equation of motion for ‘i’th and ‘j’th floquet quasienergy and corresponding floquet modes provided that T is sufficiently small to ignore the Floquet micromotions between two successive periods. Thus,

You're talking about DMBL with-out defining or explaining. Put de-scrip-tions.

$$\begin{aligned} \overline{\langle \hat{O}(nT) \rangle} &\approx \sum_{ij} \overline{e^{-i(\Omega_i - \Omega_j)nT}} O_{ij} \langle \Psi_0 | \phi_i \rangle \langle \phi_j | \Psi_0 \rangle. \\ &\approx \sum_i O_{ii} \left| \langle \phi_i | \Psi_0 \rangle \right|^2 \approx \sum_{|\phi_k\rangle \in \mathcal{S}'(\Omega_0, \delta\Omega)} O_{kk} \left| \langle \phi_k | \Psi_0 \rangle \right|^2, \end{aligned} \quad (3)$$

where the new set

$$\mathcal{S}'(\Omega_0, \delta\Omega) = \left\{ |\phi_k\rangle \ni \Omega_0 - \frac{\delta\Omega}{2} \leq \Omega_k \leq \Omega_0 + \frac{\delta\Omega}{2} \right\},$$

In this limit, drive parameters like amplitude, frequency, and duty-cycle strongly affect the  $\phi_i$ s. Thus, they can be engineered to make  $O_{kk}$  in equation 3 weakly dependent on  $|\phi_k\rangle$ , but the initial quasi energy  $\Omega_0$  heavily dependent. In particular, the functional derivative  $\frac{\delta O_{kk}}{\delta |\phi_k\rangle}$  can be made arbitrarily large. The continuum limit in eqn ?? can no longer be justified, suppressing thermalization dynamically. Thus, Floquet Engineering of quasienergies can produce Dynamical Many Body Localization (DMBL), where the system fails to reach thermal equilibrium and remains localised near its initial state even at large times. This paradigm is similar to MBL, where disorder, locality, and integrability cause athermality. Localization can occur regardless of disorder, locality of observables, or system integrability, all of which have been studied for MBL onset [15–17]. However, DMBL has been shown in integrable systems where specific drive parameters can produce additional approximate Noether charges that cause dynamical localization [6].

A paradigmatic example of an integrable system where DMBL occurs is the driven Transverse Field Ising model (TFIM) in one dimension [18]. The Hamiltonian is given by

$$\hat{H}(t) = \hat{H}_0 + h_z(t) \hat{H}_1 \quad (4)$$

$$\hat{H}_0 = -\frac{1}{2} \sum_{i=1}^N \sigma_i^x \sigma_{i+1}^x \quad (5)$$

$$\hat{H}_1 = -\frac{1}{2} \sum_{i=1}^N \sigma_i^z. \quad (6)$$

Here, the undriven Hamiltonian  $\hat{H}_0$  consists of nearest-neighbour interactions between  $N$  number of spin-1/2 particles on a one-dimensional spin network. The transverse field is denoted by  $\hat{H}_1$ , and is being modulated by a time-periodic and harmonic signal  $h_z(t) = h_0 + h \cos \omega t$ , yielding a time period  $T = 2\pi/\omega$  with amplitude  $h$ , drive frequency  $\omega$ , and d.c. field  $h_0$ . This Hamiltonian can be readily transformed into a spinless pseudo-fermionic system via the Jordan-Wigner transformation. Written in momentum space spanned by spinors  $\psi_k = (c_{-k}, c_k^\dagger)^T$  of fermions at momentum  $k$  created (annihilated) by operators  $c_k^\dagger$  ( $c_k$ ). This yields an effective Hamiltonian [4]

$$H(t) = \sum_{(k, -k)-\text{pairs}} \psi_k^\dagger \left[ \left( f_k - h_z(t) \right) \tau_z + \tau_x \Delta_k \right] \psi_k \quad (7)$$

with  $f_k = J \cos k$ ,  $\Delta_k = J \sin k$ ,  $\tau_{xyz}$  are the three Pauli Matrices, and the sum is over distinct  $(k, -k)$  Cooper Pairs. The transformation to the rotated frame

is achieved by means of the unitary transformation operator denoted as  $U(t) = \prod_k U_k(t)$ , where  $U_k(t) = \exp \left\{ \left[ \frac{i\hbar}{\omega} \sin \omega t \right] \tau_z \right\}$ . The resulting Hamiltonian is obtained through transformation,

$$H'(t) = \sum_{(k, -k)-\text{pairs}} \psi_k^\dagger \left[ \tau_z f_k + \tau_x \cos(\eta \sin \omega t) + \tau_y \cos(\eta \sin \omega t) \right] \psi_k,$$

where we defined  $\eta = 2\hbar/\omega$ . Using the Jacobi-Anger formula  $e^{i\eta \sin \omega t} = \sum_{n=-\infty}^{\infty} J_n(\eta) e^{in\omega t}$ , the transformed Hamiltonian simplifies to

$$H'(t) = \sum_{(k, -k)-\text{pairs}} \psi_k^\dagger \left[ \tau_z f_k + 2\tau_x \Delta_k \sum_{n \geq 0} J_{2n}(\eta) \cos(2n\omega t) - 2\tau_y \Delta_k \sum_{n \geq 0} J_{2n+1}(\eta) \sin((2n+1)\omega t) \right] \psi_k, \quad (8)$$

In the regime where  $\omega$  is significantly larger than  $f_k$  i.e.  $\omega \gg f_k$ , the long-term average  $\overline{H'(t)}$  can serve as a suitable approximation for  $H'(t)$ . This approximation, known as the Rotated Wave Approximation (RWA), eliminates the oscillating modes and results in an effective Hamiltonian that is independent of time.

$$H^{RWA} = \sum_{(k, -k)-\text{pairs}} \psi_k^\dagger \left[ f_k \tau_z + 2J_0(\eta) \Delta_k \tau_x \right] \psi_k, \quad (9)$$

It is evident that by manipulating the drive parameters, specifically the amplitude denoted by  $h$  and the frequency denoted by  $\omega$ , in a manner such that  $\eta$  is positioned on a root of  $J_0(\eta)$ , the fermion number can be conserved to a significant extent at this particular resonance. Consequently, it is feasible to exercise direct control over  $H^{RWA}$ , resulting in a comprehensive cessation of otherwise responsive observables. The quantification of the degree of localization or freezing of a specific (quasi) stationary state in a physically significant representation can be achieved through the utilization of the *Inverse Participation Ratio* (IPR). In the position representation, the IPR for a state  $|\psi\rangle$  [19–22] is defined as

$$\phi_{IPR} \equiv \int d\mathbf{x} |\langle \mathbf{x} | \psi \rangle|^4$$

This definition can be generalized to the IPR of a state  $|\phi\rangle$  in a representation given by complete orthonormal basis  $|m\rangle$  as

$$\phi_{IPR} \equiv \sum_m |\langle m | \psi \rangle|^4. \quad (10)$$

The smallest value of the IPR corresponds to a fully delocalized state,  $\psi(x) = 1/\sqrt{N}$  for a system of size  $N$  [22, 23]. Values of the IPR close to unity correspond to localized states [24]. For a periodically driven system, we look at the IPR of the quasi-stationary Floquet modes at  $t = T$ , where  $t = 2\pi/\omega$  for drive frequency  $\omega$ . In the TFIM model, equation 9 indicates that, at resonance, when  $J_0(\eta) = 0$ , the Floquet modes are approximately given by the fermionic Fock states, which have a trivially unit IPR in the representation of the eigenmodes of the transverse field  $\hat{H}_1$  in equation 4.

For the TFIM case, a particular Floquet mode can be decomposed into a direct product of cooper-pair states as  $|\phi\rangle = \prod_{k,-k} |\phi_k^n\rangle$ . In the RWA limit and at resonance,  $|\phi_k^n\rangle$  has values of  $|0\rangle, |k, -k\rangle$  for two values of  $n = 0, 1$  respectively. We define the reduced IPR of  $|\phi_k^n\rangle \forall k$  to be

$$\phi_{IPR}^{(n)}(k) = |\langle 0|\phi_k^n\rangle|^4 + |\langle +k, -k|\phi_k^n\rangle|^4, \quad (11)$$

where  $n = 0, 1$ . In the RWA limit and at resonance, this quantity is unity, indicating very low participation and the onset of freezing. Figure 1 shows results from numerically simulating the TFIM dynamics. The reduced IPR for a particular Floquet mode was obtained by simulating the exact Heisenberg dynamics over a single time period of the drive, and plotted as a function of momentum  $k$  for different  $\eta$ 's. At resonance, when  $\eta$  lies at the root of the Bessel function  $J_0(\eta)$ , the IPR is exactly unity for all momenta. Outside this resonance, the IPR is unity only for some momenta because the effective Hamiltonian is perfect diagonal at  $k \in \{-\pi, 0, \pi\}$  as can be seen in the cross-sectional plots of figure 1. Away from the resonance point, IPR is less than unity but as TFIM is integrable spin model, it does not follow thermalization maintaining posetive value. However, at low frequencies, when RWA fails due to unavailability of zero offdiagonal terms in the effective transformed Hamiltonian (in matrix representation) and no integrability breaking terms to counteract the off diagonal terms, the IPR remains quite high ( $IPR \sim 0.5$ ) even at resonance point as can be seen figure 2. At low frequency, this is valid for all momentum and parameter  $\eta$ , see figure 3.

Because the dependence of observable expectations on the eigenstates is always fairly strong for integrable systems like the TFIM, such systems will never exhibit any kind of thermal behaviour unless integrability breaking terms are included. As a result, it is not physically meaningful to refer to this as "Many Body Localization," because the parameter space lacks a region where ETH holds to contrast with this state. The type of Floquet Engineering described above, on the other hand, can be easily applied to a broad class of nonintegrable systems where ETH is expected to hold in certain regions. Long-range spin systems, in particular, where the exchange energies between far-off spins are taken into account in the model Hamiltonian, are good candidates because they are known to thermalize when driven with low frequencies [25].

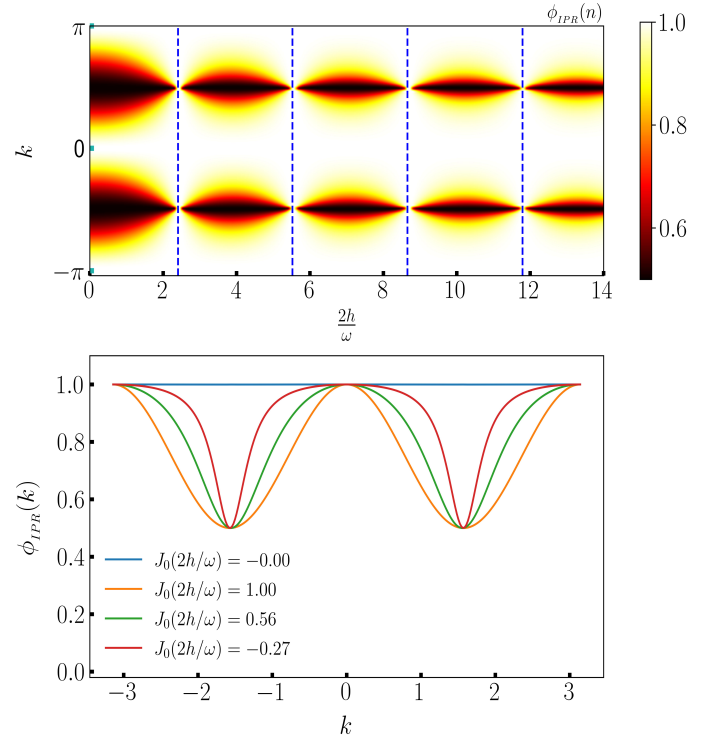


FIG. 1. The plots above are for the exact dynamics of the TFIM in Fermionic representation for size  $N = 100$ , with the reduced IPR (defined in equation 11) plotted for the entire Brillouin zone for a few drive amplitudes. The frequency is set to  $\omega = 90$  and the IPR of one of the two Floquet modes are plotted at time  $t = T$  for four different chosen amplitudes. The exact result is consistent with the RWA approximation. When  $J_0(2h/\omega) = 0$ , the RWA Hamiltonian vanishes, yielding an IPR of unity. At other points, the IPR is unity only when  $k = \pm\pi$  (since  $\Delta_k = 0$ ) and  $k = 0$  (since  $f_k = 0$  and the Hamiltonian for each  $k \sim \sigma_x$ ); other than that, there is freezing due to the ensuing dynamics.

## II. LIPKIN MESHKOV GLICK MODEL: LONG RANGE INTERACTION

The Hamiltonian of the network comprising spin 1/2 particles with Heisenberg interaction type shall be taken into consideration as below,

$$\hat{H}(t) = \hat{H}_0 + (h \cos(\omega t) + h_0) \hat{H}_1 \quad (12)$$

where

$$\begin{aligned} \hat{H}_0 &= \frac{1}{2} \sum_{ij} J_{ij} \hat{\sigma}_i^z \hat{\sigma}_j^z, \\ \hat{H}_1 &= \sum_i \hat{\sigma}_i^x. \end{aligned}$$

here,

$$J_{ij} = \frac{J_\alpha}{N^{1-\alpha}} \frac{1}{r_{ij}^\alpha}$$

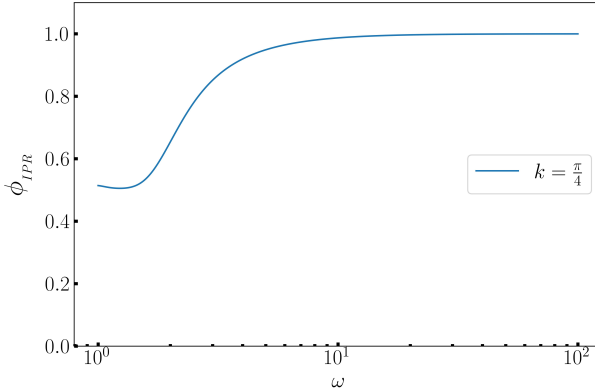


FIG. 2. IPR for TFIM is approximately 0.5 at lower frequency and 1 at higher frequency. The slow change in IPR from minimum to unity over a large frequency range indicates the absence of a mobility edge and, consequently, the absence of a phase transition. In addition, at the point of resonance at low frequency the system does not go ETH-thematization is indicated by the existence of a finite IPR.

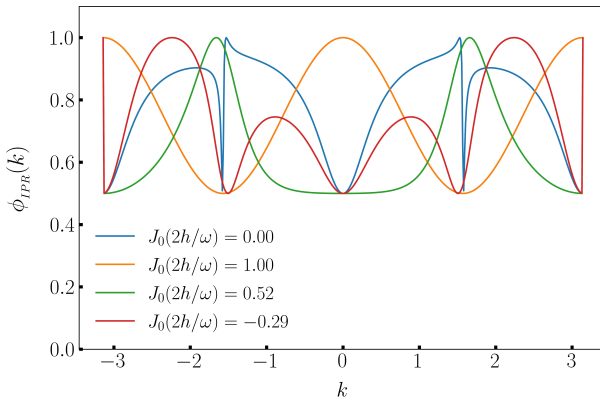


FIG. 3. A low-frequency regime  $\omega = 2.0$  plot for IPR for Ising model at four different density points for system size  $N = 500$ . IPR localization persists nonetheless.

Putting  $\alpha = 0$  yields the Lipkin Meshkov Glick (LMG) model with all-to-all interaction, yielding  $J_{ij} = J_0/N$ . We choose to maintain the extensivity of the interaction energy by enforcing the condition

$$\frac{J_0}{N} \sum_{i \neq j} 1 = \frac{J_0}{N} \frac{N(N-1)}{2} = 1$$

yielding the Kac-norm  $J_0 = 2/(N-1)$ . Here, we have  $N$  spin-1/2 particles in a 1-dimensional lattice, and  $i, j$  are site indices. The Hamiltonian in equation 12 commutes with  $P_{ij}$  with  $P_{ij}$  defined as  $P_{ij} = \frac{1}{2}(1 + \vec{\sigma}_i \cdot \vec{\sigma}_j)$ . In addition  $[S^2, H] = 0$ , therefore the  $S^2$  is invari-

ant of motion, where  $S^2 = |\vec{S}|^2$  with  $\vec{S}$  defined as,  $\vec{S} = S^x \hat{x} + S^y \hat{y} + S^z \hat{z} \equiv \frac{1}{2} \sum_i \vec{\sigma}_i$ . We now choose to populate the system in a state whose measured value of  $S^2$  is  $\frac{N}{2} \left( \frac{N}{2} + 1 \right)$ , in that case the dynamics remains invariant in the space spanned by the common eigen states of  $P_{ij}, |S|^2$  and  $S_z$ , these are also eigenstates in the so-called TSS subspace [26]. Let the eigenvalues be  $s_n$ , and the eigen vectors be  $|s_n\rangle$ , where  $s_n = -\frac{1}{2} + \frac{n}{N}$  and the index  $n = 0(1)N$  has  $N+1$  values. So, the dynamics is restricted to a  $(N \times N)$  invariant subspace where the matrix elements are given by

$$(H_0)_{ij} = -\frac{4}{N-1} s_i^2 \delta_{ij},$$

$$(H_1)_{ij} = \left[ \sqrt{\frac{N}{2} \left( \frac{N}{2} + 1 \right) - N s_i (N s_{i+1}) \delta_{i+1,j}} \right. \\ \left. + \sqrt{\frac{N}{2} \left( \frac{N}{2} + 1 \right) - N s_i (N s_{i-1}) \delta_{i-1,j}} \right] \quad (13)$$

Now we transform the Hamiltonian to the Rotated frame given by the transformation

$$\hat{U}(t) = \exp \left[ i \frac{h}{\omega} \sin(\omega t) \hat{H}_1 \right] \quad (14)$$

Defining  $\tau = \frac{h}{\omega} \sin \omega t$ , we use the fact that  $\hat{H}_1 = 2S^x$ , and the identity

$$e^{i2\tau \hat{S}^x} \hat{S}^z e^{-i2\tau \hat{S}^x} = \hat{S}^z \cos(2\tau) + \hat{S}^y \sin(2\tau) \quad (15)$$

to simplify the transformed Hamiltonian, yielding

$$\tilde{H}(t) = -\frac{1}{N-1} \left[ (S^z)^2 (1 + \cos 4\tau) + (S^y)^2 (1 - \cos 4\tau) \right. \\ \left. + \{S^y, S^z\} \sin 4\tau \right] - 2h_0 S^x \quad (16)$$

We define  $\eta \equiv 4h/\omega$  and use the Jacobi-Anger formulae [27]

$$\cos(\eta \sin \omega t) = J_0(\eta) + 2 \sum_{n=1}^{\infty} J_{2n}(\eta) \cos(2n\omega t)$$

$$\sin(\eta \sin \omega t) = 2 \sum_{n=1}^{\infty} J_{2n-1}(\eta) \sin[(2n-1)\omega t]$$

to simplify the expression for  $\tilde{H}(t)$ . It is assumed that the frequency of the drive, denoted by  $\omega$ , is sufficiently high such that all harmonic components present in the Hamiltonian can be effectively smoothed out over distinguishable time intervals. The Hamiltonian in the Rotated

Wave Approximation (RWA) is obtained as follows, neglecting constant terms in the sum.

$$\tilde{H}_{\text{RWA}} = \frac{(\hat{S}^x)^2}{N-1} - 2h_0\hat{S}^x - \frac{J_0(\eta)}{N-1} \left[ (\hat{S}^z)^2 - (\hat{S}^y)^2 \right] \quad (17)$$

If the drive amplitude  $h$  is adjusted such that  $\eta$  lies at a root of  $J_0(\eta)$  (the localization point), the RWA Hamiltonian is diagonal in the representation of the transverse field  $\hat{S}^x$ , yielding an IPR of unity in that representation, similar to the Ising case. Note however, that if the DC transverse field  $h_0$  is set to 0, then, at the localization point, the RWA Hamiltonian  $\tilde{H}_{\text{RWA}} \sim (\hat{S}^x)^2$ , each of whose eigenvalues (given by  $(\frac{N}{2} - m)^2$  where  $m \in 0(1)N$ , and  $(\frac{N}{2} - m)$  are the eigenvalues of  $\hat{S}^x$ ) are two-fold degenerate. This produces infinitely many (Floquet) eigenmodes in the degenerate subspace whose IPRs may not always be unity in the  $S^x$  representation. Thus, the absence of the DC field may produce delocalization in the Floquet states even at the localization points, and this necessitated the inclusion of a DC field  $h_0$  in order to break the symmetry. Finally, note that not all values of the DC field  $h_0$  remove all degeneracies in  $\tilde{H}_{\text{RWA}}$ . To see this, note that, at the localization point, the eigenvalues of  $\tilde{H}_{\text{RWA}}$  are given by

$$\text{Eigs}\left[\tilde{H}_{\text{RWA}}\right] = \frac{\left(\frac{N}{2} - m\right)^2}{N-1} - 2h_0\left(\frac{N}{2} - m\right) \quad (18)$$

In order to ensure that no degeneracies occur, we have to adjust  $h_0$  to ensure that for any two integers  $m_1, m_2 \leq N$  the condition following is always met,

$$\frac{\left(\frac{N}{2} - m_1\right)^2}{N-1} - 2h_0\left(\frac{N}{2} - m_1\right) \neq \frac{\left(\frac{N}{2} - m_2\right)^2}{N-1} - 2h_0\left(\frac{N}{2} - m_2\right) \quad (19)$$

If  $N \gg 1$  (substantially large), then this condition can be met by assuring that  $(1 - 2h_0)^{-1}$  is never an integer that is divisible by  $N$ . To ensure this in our numerical simulations we have kept  $h_0$  at a small irrational value.

This result is supported by exact numerical results, as can be seen in the plots below in FIG. 4. There, we show plots of the IPR of the Floquet mode  $|\phi\rangle$  for all  $n$  corresponding to eigenvalues of  $S^x$  for a fixed eigenvalue of  $S^2 = N/2(N/2 + 1)$ . The IPR is thus

$$\phi_{\text{IPR}}(n) = \sum_m |\langle m | \phi^n \rangle|^4 \quad (20)$$

where  $|m\rangle$  is the  $m^{\text{th}}$  eigenstate of  $\hat{S}^x$ .

Now, we focus at numerical simulations for  $H(t)$  via the IPR of the Floquet state in the representation of the transverse field i.e. the eigenstates of  $S^x$ . We kept  $\omega = 90$  as a large enough value for RWA to hold, and  $N = \mathcal{O}(10^2)$  which our standard computational resources will allow.

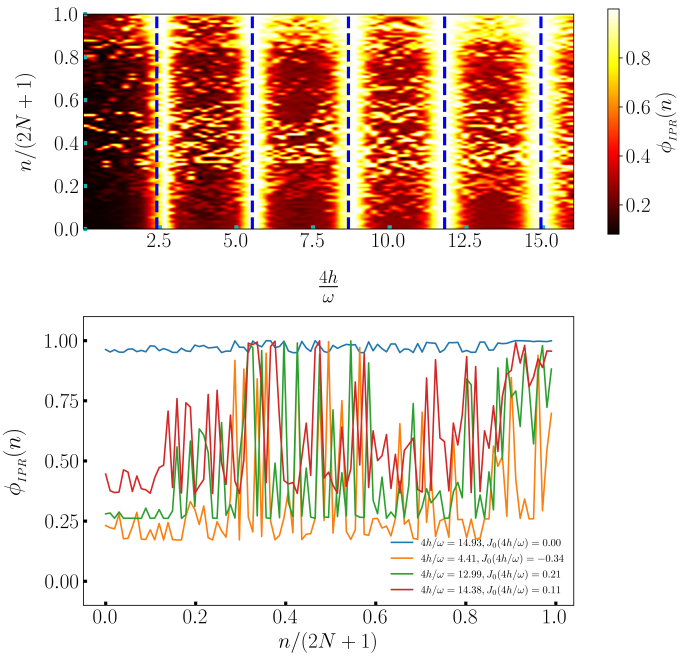


FIG. 4. The IPR for exact dynamics for spin model size  $N \sim 30$ . The upper panel shows a density plot of the IPR of Floquet modes for different parameter points corresponding to the ratio between strength and the frequency of the symmetry-breaking field which is the lowest root among Bessel's roots of the first kind and zeroth order  $\frac{4h}{\omega}$ . The dc part of the symmetry-breaking field is kept at a small irrational number to avoid the symmetry arising from degeneracy in Flqouet states. The IPR density is high at Bessel's first order roots,  $J_0\left(\frac{4h}{\omega}\right) = 0$  for all the available floquet states. The lower panel shows a crossectional plot of IPR for four different floquet IPR density points. The point corresponding  $J_0\left(\frac{4h}{\omega}\right) = 0$  has unity value for all states where points away from the roots have lower and high fluctuations.

The uppermost section displays a density plot that depicts the Inverse Participation Ratio (IPR) of the Floquet states. The abscissa represents  $\eta = 4h/\omega$ , while the ordinate represents the spin index  $m/(2N+1)$ . The vertical lines that are dashed and colored blue correspond to the roots of the Bessel function of the first kind with order zero, denoted as  $J_0(\eta)$ . Evidently, the Inverse Participation Ratio (IPR) approaches a value of one for high values of the root of the Bessel function  $J_0(\eta)$ , which suggests a state of full localization of the Many Body system. Nevertheless, a deviation from unity occurs at the smallest root of  $J_0(\eta)$ . The observed phenomenon can be attributed to the fact that when  $\eta$  approaches the smallest root of  $J_0(\eta)$ , which is approximately equal to 2.405, the amplitudes of the higher order terms in the RW expansion, denoted by  $\mathcal{O}(J_n(\eta))$ , become significant enough to contribute to the process of delocalization. Thus, a greater magnitude of the root is favored for the purpose of investigating the phenomena.

The bottom panel contains cross sections of the full IPR plot for selected values of  $\eta$  as indicated in the legend. When the drive amplitude  $h$  is adjusted to make  $J_0(\eta) \neq 0$ , the Floquet States are mixed, but not entirely thermal, since the IPR does not fall to  $\mathcal{O}(N^{-1})$ , indicating that localization persists to some extent always.

So, as long as there is an appropriate DC field,  $S^x$  is mostly conserved and  $H_F$  is mostly diagonal in the

$S^x$  representation at the freezing point. The small deviations from this conservation occur due to the role of higher order terms in the Fourier expansion of the Hamiltonian on the rotating basis that contribute additional time-periodic terms to the RWA Hamiltonian, as can be seen in FIG.II.

The full Hamiltonian for the LMG model on the rotated basis is

$$\begin{aligned} \tilde{H}^{RWA}(t) \sim & \frac{(\hat{S}^x)^2}{N-1} - 2h_0\hat{S}^x - \frac{J_0(\eta)}{N-1} \left[ (\hat{S}^z)^2 - (\hat{S}^y)^2 \right] - \frac{2}{N-1} \sum_{n=1}^{\infty} J_{2n}(\eta) \left[ (\hat{S}^z)^2 - (\hat{S}^y)^2 \right] \cos(2n\omega t) \\ & - \frac{2}{N-1} \sum_{n=1}^{\infty} J_{2n-1}(\eta) \{ \hat{S}^y, \hat{S}^z \} \sin[(2n-1)\omega t] \end{aligned} \quad (21)$$

The IPR plots pertaining to exact dynamics indicate that the freezing point, represented by the initial blue curve corresponding to Bessel's root of zeroth order of first kind, is insufficient for achieving many-body localization, as depicted in the top panel. The reason for this phenomenon is attributed to the greater magnitude of other Bessel roots of higher order, which in turn leads to delocalization. However, it is worth noting that at elevated localization points (as depicted by the dashed orange curve), localization is particularly conspicuous. In terms of system distribution, a range of curves, denoted by both green and red, illustrates the degree of distribution. The zeroth order RWA in the central panel exhibits a consistent pattern at locations distant from the resonance point, as evidenced by the congruent green and red curves. However, the curves for both higher and lower localization points display complete localization, which contradicts the precise findings presented in the top panel. This necessitates the incorporation of higher-order corrections into the Rotating Wave Approximation (RWA). The application of the first-order correction to the Rotating Wave Approximation (RWA) in the lower panel results in a curve structure that is recognizable and consistent with the exact dynamics.

### III. CLASSICAL LIPKIN DYNAMICS

In the context of the classical (continuum) limit, where  $N$  approaches infinity, the disparity between neighboring values of  $s_i$  in equation 13 can be disregarded, resulting in a Hamiltonian per particle of  $h(t) \equiv \frac{1}{N}$  and the Hamiltonian per particle becomes

$$h(t) = \frac{1}{N} H(t) = h + h_0 \cos(\omega t) h_1, \quad (22)$$

where,

$$\begin{aligned} (h)_{ij} &\approx -2s_i^2 \delta_{ij}, \\ H_0 &\rightarrow -2s^2 \\ (h_1)_{ij} &\approx \sqrt{1-4s_i^2} [\delta_{i+1,j} + \delta_{i-1,j}] \\ H_1 &\rightarrow \sqrt{1-4s_i^2} \cos p, \end{aligned} \quad (23)$$

In the continuum limit, the Lipkin system can be described by  $p, q$  with corresponding Hamiltonian [28]:

$$H = -2q^2 - h(t) \sqrt{1-4q^2} \cos p, \quad (24)$$

which yields the Hamiltonian dynamical system

$$\begin{aligned} \frac{dq}{dt} &= h(t) \sqrt{1-4q^2} \sin p \\ \frac{dp}{dt} &= 4q \left[ 1 - \frac{h(t) \cos p}{\sqrt{1-4q^2}} \right] \end{aligned} \quad (25)$$

We solved Hamiltonian numerically 24 using equations 25 to obtain position and momentum coordinates  $p, q$  and plotted in the Poincaré surface of section (PSOS) strobed at each multiple of time period. A chaotic Poincare pattern is found for all small drive amplitude s.t.  $A/J < 0.5$  and also a regular pattern emerges at for ratios  $A/J \geq 0.5$  both at small drive frequency  $\omega \sim 2.0$  [25].

However, under a regime of sufficiently high frequency, the system exhibits distinct behavior. The study involves a comparison of the Poincaré sections of the ensuing dynamics under the influence of  $h(t) = h \cos \omega t$ , where two distinct scenarios have been considered. The first scenario pertains to the case where  $\omega = 2.5$ , corresponds to a lower frequency and, consequently, a smaller amplitude. The second scenario pertains to the case where  $\omega = 90.0$ , corresponds to a higher frequency

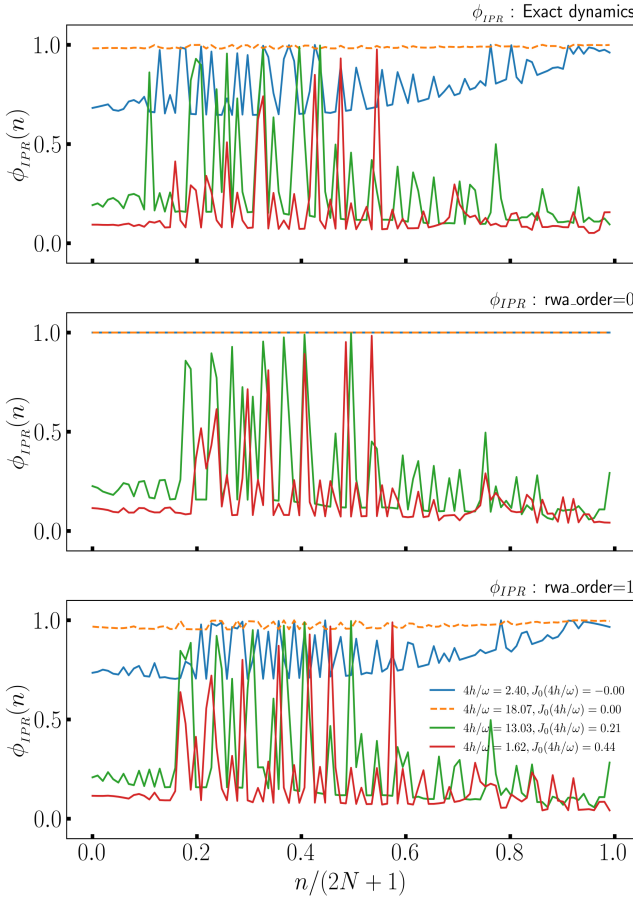


FIG. 5. The comparison between IPR for exact dynamics and RWA with corresponding correction orders. IPR is calculated for four different  $\eta$ 's and corresponding  $J_0(\eta) \neq 0$  values for colors, Blue : $\eta = 2.40, J_0(\eta) = 0.0$ , dashed orange: $\eta = 18.07, J_0(\eta) = 0.0$ , Green: $\eta = 13.03, J_0(\eta) = 0.21$ , Red: $\eta = 1.62, J_0(\eta) = 0.44$ . IPR plots for RWA with zeroth order aren't enough to describe the exact dynamics, but plots for RWA with first-order correction are similar to the exact dynamics.

and, correspondingly, a higher amplitude. Both scenarios have been evaluated at  $J_0(4h/\omega) = 0$ . The Husimi Q-functions of the acquired Floquet States are compared with these. The quantum phase space is characterized by the Spectral Average of the Husimi functions of all the Floquet modes  $|\phi^n\rangle$  for a given value of  $S^2$ . Specifically, for a coherent state  $|q, p\rangle$ , the corresponding plot is presented in FIG.6.

$$H(q, p) \equiv \frac{1}{(2N+1)\pi} \sum_n \langle q, p | \phi^n \rangle \langle \phi^n | q, p \rangle$$

The classical plots are dominated by chaos at low values of  $\omega$ , as noted in Kidd's work [29]. Conversely, at high values of  $\omega$ , the Poincaré plot exhibits a distinct regular pattern, indicating localization.

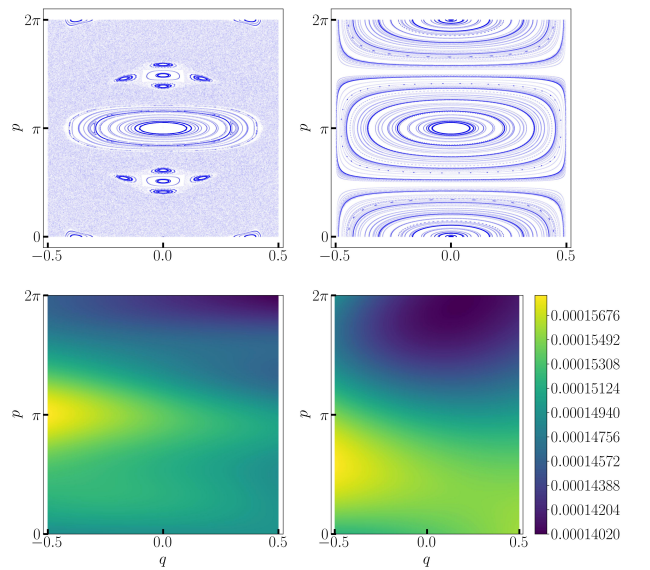


FIG. 6. The above panel describes the phase-space Poincaré distribution symmetry breaking smaller drive frequency  $\omega = 2.5$  (left) and higher frequency  $\omega = 90.0$  (right) for system size  $N = 500$  with 100 realisation numbers. At smaller frequencies, the Poincaré picture contains chaotic behaviour (top left panel) whereas at the higher frequencies, it is a normal Poincaré picture which represents discrete freezing behaviour (top right panel). The bottom panel is Husimi Q-function average plot for a smaller frequency (bottom left) and has a uniform distribution with less contrast in colour. This means a Q-function distribution in chaotic behaviour. At the right bottom, the Husimi plot has distinct colour contrast in the Q-function average value which represents a regular dynamics pattern in the system.

#### IV. THERMALITY TO ATHERMALITY: A PHASE CROSSOVER

The analysis of the Lipkin-Glick-Meshkov model reveals two distinct scenarios at low and high external drive frequencies. As a result, it is hypothesized that a change in phase may occur due to the influence of frequency. IPR of the Floquet modes is computed numerically and plotted in FIG.7 for numerous frequencies in ascending order from frequency  $\omega = 1.0$  upto  $\omega = 50.0$  so that the system can vary adiabatically, along with the associated drive amplitude  $h$  for the localization resonant point, which is  $J_0\left(\frac{4h}{\omega}\right)$  (Top panel). In the low-frequency range spanning from  $\omega = 1.0$  to approximately  $\omega \approx 9.0$ , the Inverse Participation Ratio (IPR) exhibits values below unity. Moreover, the IPR gradually diminishes with increasing system size, following a  $\frac{1}{N}$  trend, which confirms the participation distribution (as shown in the bottom panel). As the limit of  $N$  approaches infinity, the inverse participation ratio (IPR) tends towards zero, indicating a fully

delocalized state. The study conducted by IPR revealed a gradual increase in the unity of IPR over a certain frequency range, specifically at approximately  $\omega = 5.0$ . The increase in intellectual property rights (IPR) is not characterized by a sudden surge, but rather a gradual increase that exhibits a phase crossover. As the size of the system increases, the crossover region becomes smoother.

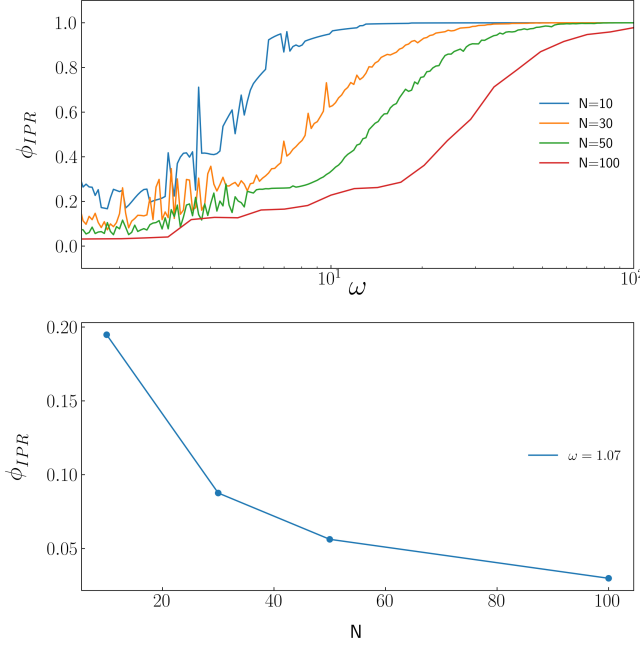


FIG. 7. The plotting of the Inverse Participation Ratio (IPR) at Bessel's first root with first kind  $J_0\left(\frac{4h}{\omega}\right)$  for varying drive amplitudes and frequencies in a spin array of LMG type, for different spin sizes  $N = 10, 30, 50, 100$ . The adiabatic increase of the drive frequency is observed in the range of  $O(1)$  to  $O(50)$  for varying system sizes of  $N = 10, 30, 50$ , and  $100$ . The study reveals that the IPR exhibits a decrease in magnitude at low frequencies, followed by an increase to unity at high frequencies, across various system sizes (top panel). The findings indicate that the system's inverse participation ratio (IPR) diminishes in proportion to  $N$  in low-frequency regions, thereby validating the distribution of the system's state participation, as demonstrated in the lower panel. The increase in the instantaneous power reserve (IPR) with respect to system frequency exhibits a consistently gradual trend until it reaches a high frequency where IPR is unity, which is contingent upon system parameters. The lower panel indicates that the IPR decreases proportionally with the system size, which can be attributed to the distribution of states at lower frequencies.

The numerical evolution of the system is carried out using the exact Hamiltonian for a duration of 500 time periods. The average of the Hamiltonian, denoted as  $\langle H \rangle$ , is then computed to determine the energy spreading through the standard deviation. The thermal conditions necessitate minimal fluctuations in energy distribution, as the spread of states leads to a limited standard

deviation[30]. As a result, finite standard deviation arises in athermal regions. A graph depicting the standard deviation of the energy expectation value is presented for a system Hamiltonian adiabatically varied with drive frequency. The standard deviation of the Hamiltonian, denoted as  $\langle H \rangle_{std}$ , exhibits a small value for frequencies up to approximately  $\omega \sim 5.0$ . Subsequently, there is an increase in that follows a linear pattern as the frequency increases further  $\langle H \rangle_{std} \propto \omega$ . A thermal region is observed at a lower frequency, while an athermal region is detected at a higher frequency.

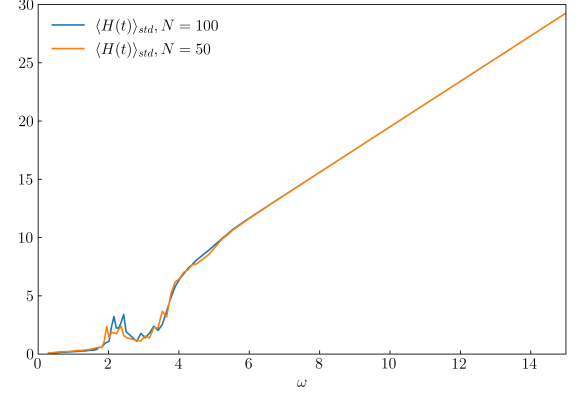


FIG. 8. The standard deviation of the mean value of  $H$ , denoted by  $\langle H \rangle_{std}$ , has been calculated over a span of 500 time periods. A singularity has been identified at approximately  $\omega = 5.0$ . The standard expectation value of the Hamiltonian, denoted as  $\langle H \rangle_{std}$ , exhibits a diminutive magnitude below the singularity, while a linear and gradual augmentation is observed at higher frequencies. A small standard deviation indicates the presence of a thermal region, whereas a larger finite standard deviation suggests the existence of a regular athermal region.

## V. OBSERVATIONS AND DISCUSSION

The quantum many-body localization in the Ising model is observed at high drive frequency and corresponding high drive amplitude, where the localization points are determined by setting  $J_0(2h/\omega) = 0$  for both exact and Rotated wave simulations. The delocalization away from the localization points is relatively weak. The integrability of the Ising model allows for localization to be observed at low values of  $\omega$ , despite the breakdown of the rotating wave approximation. Analytical methods beyond the adiabatic limit are intricate. The LMG model exhibits distinct localization at localization points, which are determined by the condition  $J_0(4h/\omega) = 0$ , in both the exact and Rotated Wave simulations. However, there is some degree of delocalization observed beyond these points, albeit weak. The non-integrability of the LMG model and the established onset of chaos in the

thermodynamic limit at low  $\omega$  lead to a near-complete delocalization in the Inverse Participation Ratio (IPR) of the Floquet states at small  $\omega$ .

Consequently, we adiabatically varied  $\omega, h$  in the LMG model, under the constraint that  $\eta = 4h/\omega$  was held at a root of  $J_0(\eta)$ . There, we observed a crossover or phase change from nearly fully thermal to completely localised behaviour (see FIG.7). Even if the limitation is relaxed, the macroscopic behaviour changes from thermal to athermal. At low frequencies, IPR is observed to decrease with increasing system size  $N$ , and when  $N$  is big, i.e.,  $\rightarrow \infty$ , IPR appears to evaporate, resulting in a fully thermalized state at  $\eta = 4h/\omega$ . This is in contrast to the Ising model, which lacks such a transition. Thus, the incorporation of long-range interactions appears to trigger a transition from the thermal phase to the localised phase, a property that will prove useful in the design of MBL engines.

## VI. CONCLUSION AND OUTLOOK

The study delved into the onset of Dynamical Many-Body Localization in the Lipkin-Glick-Meshkov spin model, specifically in regularly driven long-range spins, serving as a paradigmatic illustration. The parametrization of many-body localization is based on the Inverse Participation Ratio of the Floquet eigenstates. The present study conducted a numerical comparison between the inverse participation ratio (IPR) of the LMG model and the transverse field Ising model (TFIM) at both low and high drive frequencies. The present study involved an examination of the phase space dynamics of the LMG model. Specifically, we sought to analyze the emergence of thermal behavior at low frequencies and localization at high frequencies, as well as the appearance of additional approximately conserved quantities in the high-frequency regime for both models.

*Conclusion:* Long-range spins exhibit strong localization in spin-coordinate space for the LMG model when the drive frequency is  $\omega \gg J$ , where  $J$  represents the spin exchange energy. The localization of the LMG model occurs at specific resonances of the drive frequency  $\omega$  and amplitude  $h$ , where  $J_0(4h/\omega) = 0$ . The TFIM case has shown comparable localization (in momentum space) at resonances determined by  $J_0(2h/\omega) = 0$ . However, the mechanism differs in long-range systems as a distinct observable  $(S_x)^2$  is conserved in the LMG case, where  $\mathbf{S}$  represents the total spin. Upon the removal of accidental degeneracy through the application of a DC trans-

verse field in the form of  $\sim \hat{S}_x$ , the eigenstates can be mapped into a coordinate representation, leading to a robust spatial localization. The periodically driven LMG model exhibits a pronounced mobility edge when the frequency is gradually increased from  $\omega \sim J$  to  $\omega \gg J$  in an adiabatic manner. In the first region where frequency  $\omega$  is small, the quantum system is expected to undergo thermalization at exceedingly high temperatures due to the attainment of dynamical chaos in classical dynamics. However, in the latter high frequency regime, the perpetual postponement occurs due to dynamical localization. The point of transition in mobility between these two regimes exhibits anomalous characteristics when analyzed in the context of thermodynamic principles, indicating a quantum phase transition between them. The absence of thermal behavior in the low-frequency limit of the short-range transverse field Ising model (TFIM) can be attributed to the significant magnitude of the inverse participation ratio (IPR). The induction of Thermal and Localized states in long-range systems can be achieved through Floquet engineering, without the need for disorder.

*Outlook:* A system characterized by high symmetry has been thoroughly examined in a pristine state. Thermalization takes place in all scenarios, alongside integrability-disrupting factors, such as disorder. However, akin to the transverse field Ising model (TFIM), the onset of thermalization in the Lipkin-Meshkov-Glick (LMG) model can be postponed when the condition  $\omega \gg J$  and  $J_0(4h/\omega) = 0$  is satisfied. In systems possessing a Hamiltonian of the form  $\mathcal{H} = -\frac{J_{ij}}{|i-j|^\beta} \sum_{ij} \sigma_i^z \sigma_j^z - \sum_i \sigma_i^x$ , the time-independent Schrödinger equation can be solved analytically for certain potentials. The expression above represents the summation of the product of the coupling constant  $J_{ij}$  and the difference between the indices  $i$  and  $j$  raised to the power of  $\beta$ , multiplied by the sum of the spin variables sigma over all possible pairs of indices  $i$  and  $j$ . The intermediate spin-spin interaction power law limits have received less attention compared to the infinite and long-range limit. Further research can be conducted on this topic. The LMG spin configuration undergoes a phase transition due to the adiabatic increase in drive frequency. This suggests the possibility of a future MBL engine that can operate between the thermal and localized regimes, with a thermodynamic cycle. Additionally, there exist prospects for diabatic corrections.

*Acknowledgement:* One of the authors, MR would like to express gratitude to The University of Burdwan for awarding the state-funded fellowship and facilitating access to advanced computational resources.

- 
- [1] P. Bordia, H. Lüschen, U. Schneider, M. Knap, and I. Bloch, Periodically driving a many-body localized quantum system, **13**, 460.
  - [2] S. Sahoo, I. Schneider, and S. Eggert, Periodically driven

- many-body systems: A floquet density matrix renormalization group study, .
- [3] A. Das, Exotic freezing of response in a quantum many-body system, **82**, 172402.

- [4] G. B. Mbeng, A. Russomanno, and G. E. Santoro, The quantum ising chain for beginners, 2009.09208 [cond-mat, physics:quant-ph].
- [5] H. S. Yamada and K. S. Ikeda, Localization and delocalization properties in quasi-periodically-driven one-dimensional disordered systems, **105**, 054201.
- [6] A. Roy and A. Das, Fate of dynamical many-body localization in the presence of disorder, **91**, 121106 ().
- [7] A. Campa, T. Dauxois, and S. Ruffo, Statistical mechanics and dynamics of solvable models with long-range interactions, **480**, 57.
- [8] T. Eisele and R. S. Ellis, Multiple phase transitions in the generalized curie-weiss model, **52**, 161.
- [9] A. Canning, A class of long range ising spin models described by curie-weiss mean field theory, **185**, 254.
- [10] G. Misguich, V. Pasquier, and J.-M. Luck, Inverse participation ratios in the xxz spin chain, Phys. Rev. B **94**, 155110 (2016).
- [11] M. Calixto and E. Romera, Inverse participation ratio and localization in topological insulator phase transitions, **2015**, P06029.
- [12] K. Fujii, Introduction to the rotating wave approximation (RWA): Two coherent oscillations, **8**, 2042.
- [13] L. Reichl, *The Transition to Chaos: Conservative Classical and Quantum Systems*, Fundamental Theories of Physics, Vol. 200 (Springer International Publishing).
- [14] M. Bukov, L. D'Alessio, and A. Polkovnikov, Universal High-Frequency Behavior of Periodically Driven Systems: from Dynamical Stabilization to Floquet Engineering, ArXiv: 1407.4803v2.
- [15] S. Rozhin, Abolfazl, Floquet-induced localization in long-range many-body systems 10.1103/PhysRevResearch.5.013094.
- [16] L. N. Alet Fabien, Many-body localization: An introduction and selected topics 10.1016/j.crhy.2018.03.003.
- [17] S. J. Garratt and S. Roy, Resonant energy scales and local observables in the many-body localized phase, **106**, 054309, publisher: American Physical Society.
- [18] R. B. Stinchcombe, Ising model in a transverse field. i. basic theory, **6**, 2459.
- [19] S. Mukherjee, A. Spracklen, D. Choudhury, N. Goldman, P. Öhberg, E. Andersson, and R. R. Thomson, Modulation-assisted tunneling in laser-fabricated photonic wannier–stark ladders, **17**, 115002, publisher: IOP Publishing.
- [20] S.-H. Lin, B. Sbierski, F. Dorfner, C. Karrasch, and F. Heidrich-Meisner, Many-body localization of spinless fermions with attractive interactions in one dimension, **4**, 002.
- [21] N. C. Murphy, R. Wortis, and W. A. Atkinson, Generalized inverse participation ratio as a possible measure of localization for interacting systems, **83**, 184206, publisher: American Physical Society.
- [22] E. J. Torres-Herrera, I. Vallejo-Fabila, A. J. Martínez-Mendoza, and L. F. Santos, Self-averaging in many-body quantum systems out of equilibrium: Time dependence of distributions, **102**, 062126, publisher: American Physical Society.
- [23] N. Trivedi and D. Heidarian, Can disorder drive a mott insulator into a metal in 2d?, **160**, 296.
- [24] G. Misguich, V. Pasquier, and J.-M. Luck, Inverse participation ratios in the XXZ spin chain, **94**, 155110, publisher: American Physical Society.
- [25] A. Russomanno, R. Fazio, and G. E. Santoro, Thermalization in a periodically driven fully connected quantum ising ferromagnet, **110**, 37005.
- [26] T. Mori, Prethermalization in the transverse-field ising chain with long-range interactions, **52**, 054001, publisher: IOP Publishing.
- [27] F. E. H. George Arfken, Hans Weber, *Mathematical Methods for Physicists*.
- [28] B. Sciolla and G. Biroli, Quantum quenches and off-equilibrium dynamical transition in the infinite-dimensional bose-hubbard model, **105**, 220401.
- [29] R. A. Kidd, M. K. Olsen, and J. F. Corney, Quantum chaos in a bose-hubbard dimer with modulated tunneling, Phys. Rev. A **100**, 013625 (2019).
- [30] P. Reimann, Symmetry-prohibited thermalization after a quantum quench, **2021**, 103106, publisher: IOP Publishing and SISSA.
- [31] A. Roy and A. Das, Fate of dynamical many-body localization in the presence of disorder, **91**, 121106 ().
- [32] N. Srivatsa, R. Moessner, and A. E. Nielsen, Many-body delocalization via emergent symmetry, **125**, 240401.
- [33] Quantum ising phase transition.
- [34] B. Marcos, A. Gabrielli, and M. Joyce, Relaxation of quasi-stationary states in long range interacting systems and a classification of the range of pair interactions, **10**, 676.
- [35] A. Haldar and A. Das, Dynamical many-body localization and delocalization in periodically driven closed quantum systems, **529**, 1600333.
- [36] N. Yunger Halpern, C. D. White, S. Gopalakrishnan, and G. Refael, Quantum engine based on many-body localization, **99**, 024203.
- [37] J. M. Deutsch, Quantum statistical mechanics in a closed system, **43**, 2046 ().
- [38] M. Srednicki, Chaos and quantum thermalization, **50**, 888.
- [39] E. W. Hobson, On the Second Mean-Value Theorem of the Integral Calculus (1909).
- [40] M. Srednicki, The approach to thermal equilibrium in quantized chaotic systems, Journal of Physics A: Mathematical and General **32**, 1163 (1999).
- [41] M. Rigol and M. Srednicki, Alternatives to eigenstate thermalization, Physical Review Letters **108**, 10.1103/physrevlett.108.110601 (2012).
- [42] J. M. Deutsch, Eigenstate thermalization hypothesis, **81**, 296 ().
- [43] R. Nandkishore and D. A. Huse, Many-body localization and thermalization in quantum statistical mechanics, Annual Review of Condensed Matter Physics **6**, 15 (2015), <https://doi.org/10.1146/annurev-conmatphys-031214-014726>.